Vol. 18, No. 2 (2019) 581-588

Revista Mexicana de Ingeniería Química

THEORETICAL AND EXPERIMENTAL STUDY OF DIFFERENT CHEMICAL ROUTES TO SYNTHESIZE CRYSTALLINE SODIUM METASILICATE FROM SILICA-RICH SAND

ESTUDIO TEÓRICO Y EXPERIMENTAL DE DIFERENTES RUTAS QUÍMICAS PARA SINTETIZAR METASILICATO DE SODIO CRISTALINO A PARTIR DE ARENA RICA EN SÍLICE

A. Tejeda-Ochoa[1,2], C. Carreño-Gallardo[1], J.E. Ledezma-Sillas[1], C. Prieto-Gomez[3], N.R. Flores-Holguin[1], F.C. Robles-Hernandez[2], J.M. Herrera-Ramirez[1,2]*

[1]*Centro de Investigacion en Materiales Avanzados (CIMAV), Laboratorio Nacional de Nanotecnologia, Miguel de Cervantes 120, 31136 Chihuahua, Chih., Mexico.*

[2]*Department of Mechanical Eng. Tech., University of Houston, Houston, TX 77204-4020 USA.*

[3]*Grupo Cementos de Chihuahua (GCC), Nombre de Dios S/N, 31110 Chihuahua, Chih., Mexico.*

Received: December 9, 2018; Accepted: February 14, 2018

Abstract

Sodium silicate has a wide range of applications such as adhesives, lower carbon cements, cleaning compounds, deflocculants, protective coatings, soaps and detergents, silica-type catalysts and gels, and pigments. It is mainly obtained as a liquid, but a small fraction can be found in solid state. In this work, three different synthesis methods to produce crystalline sodium metasilicate are analyzed; the importance of synthesizing it in powder form is to be able to incorporate it into the productive processes of the cement industry, whose equipment is made for this purpose. Silicon dioxide in stoichiometric ratio was combined with each one of the following reactants: $NaHCO_3$, Na_2CO_3 and NaOH. We present the most effective synthesis route to obtain sodium metasilicate based on a computational analysis and the results are validated experimentally. The characterization was carried out by X-ray diffraction and the Rietveld refinement, as well as by calorimetry and infrared and Raman spectroscopies. The experimental results, as well as that of the molecular simulation, indicate that the most effective reaction is by using Na_2CO_3 as a reactant. Furthermore, it was possible to obtain granular crystalline sodium metasilicate, which is ideal for the production of lower carbon cements.

Keywords: Sodium metasilicate; FTIR, Raman spectroscopy, thermal analysis; molecular simulation.

Resumen

El silicato de sodio tiene una amplia gama de aplicaciones, tales como adhesivos, cementos de bajo contenido de carbono, compuestos de limpieza, defloculantes, recubrimientos protectores, jabones y detergentes, catalizadores y geles de tipo sílice y pigmentos. Es obtenido principalmente como líquido, pero en una pequeña fracción se puede encontrar en estado sólido. En este trabajo, se analizan tres métodos de síntesis diferentes para producir metasilicato de sodio cristalino; la importancia de sintetizarlo en forma de polvo es poder incorporarlo a los procesos productivos de la industria del cemento, cuyos equipos están hechos para este propósito. Se combinó dióxido de silicio en proporción estequiométrica con cada uno de los siguientes reactivos: $NaHCO_3$, Na_2CO_3 y NaOH. Presentamos la ruta de síntesis más eficaz para obtener metasilicato de sodio basado en un análisis computacional y los resultados fueron validados experimentalmente. La caracterización se llevó a cabo mediante difracción de rayos X y refinamiento Rietveld, así como por calorimetría y espectrometrías de infrarrojo y Raman. Los resultados experimentales, así como los de simulación molecular, indican que la reacción más efectiva es empleando Na_2CO_3 como reactivo. Además, fue posible obtener metasilicato de sodio cristalino en forma granular, el cual resulta ideal para la producción de cementos de bajo contenido de carbono.

Palabras clave: Metasilicato de sodio; espectroscopía de infrarrojo, espectroscopía Raman, análisis térmico; simulación molecular.

* *Corresponding author. E-mail*: martin.herrera@cimav.edu.mx
Tel. 01-61-44-39-48-27

https://doi.org/10.24275/uam/izt/dcbi/revmexingquim/2019v18n2/Tejeda
issn-e: 2395-8472

1 Introduction

Sodium silicate is a generic name for chemical compounds with the formula $Na_{2x}SiO_{2+x}$, which are highly hygroscopic inorganic substances. Similar to sodium chloride (NaCl), sodium silicate is a completely water-soluble material available from suppliers in a wide range of water contents and other compounds such as silica (SiO_2) and sodium oxide (Na_2O) (Brown & Limited, 1994). Sodium silicate generally consists of a mixture of metasilicate (Na_2SiO_3), dimetasilicate ($Na_2Si_2O_5$) and orthosilicate (Na_4SiO_4) (Bulatovic, 2007).

The Na_2SiO_3 is produced by different methods and procedures. For instance, melting is a process where a mixture of sodium bicarbonate ($NaHCO_3$) and silica (SiO_2) are heated to 1200-1400 ºC, followed by cooling for 10-12 min to reach temperatures between 600 and 800 ºC. The Na_2SiO_3 product is usually crystalline that is milled to particle sizes of 1 mm (Rehren, 2000; Schimmel, 1993b). Another method is the melting of sodium carbonate (Na_2CO_3) and SiO_2 at the same range of temperatures. In this case, the product is an amorphous glass (NOM, 2009). At lower temperatures (180-240 ºC), Na_2SiO_3 is produced using SiO_2 and sodium hydroxide (NaOH) in an autoclave at pressure from 1 to 3 MPa. The resulting product is an amorphous material with a water content between 15 and 23 wt% (Schimmel, 1993a).

The aim of this work was to determine the most effective reaction by comparing three different routes, in order to obtain crystalline sodium metasilicate in powder form, which could be used in the production of lower carbon cements (Torres-Ochoa, Osornio-Rubio, Jiménez-Islas, Navarrete-Bolaños, & Martínez-González, 2019), silica-type catalysts (Daramola, Nkazi, & Mtshali, 2015), zeolites (López *et al.*, 2018), deflocculants (Evcin, 2011), etc. In this research, molecular modelling was used as a complementary approach to support our findings. The theoretical work was supported by means of density functional theory (DFT) model based on the theorems of Hohenberg and Kohn (Hohenberg & Kohn, 1964). The thermodynamic constants used in this work were calculated experimentally using differential scanning calorimetry (DSC). Last, the analytical work was then validated experimentally.

2 Materials and methods

The methodology was divided in two parts: computational analysis and experimental procedure.

2.1 Computational analysis

2.1.1 Characterization

Three different reactions were defined to obtain sodium metasilicate, as shown by Eqs. (1)-(3).

$$2\,NaHCO_3(s) + SiO_2(s) \xrightarrow{\Delta} Na_2SiO_3(s) + H_2O(g) + 2\,CO_2(g) \quad (1)$$

$$Na_2CO_3(s) + SiO_2(s) \xrightarrow{\Delta} Na_2SiO_3(s) + CO_2(g) \quad (2)$$

$$2\,NaOH(s) + SiO_2(s) \xrightarrow{\Delta} Na_2SiO_3(s) + H_2O(g) \quad (3)$$

The molecular systems were classified as reactants and products in each case. The characterization was carried out by the density functional theory (DFT) model (Parr, 1980) and the time-dependent (TD) DFT (Stratmann, Scuseria, & Frisch, 1998) in the Gaussian 09 program (Frisch *et al.*, 2009) using the GaussViewW 5.08 graphics interface. After a methodology validation, the hybrid-meta-GGA functional considered in this study was the M062X (Zhao & Truhlar, 2008). A base assembly LanL2DZ (Schaefer, 2013) was used to develop the geometrical optimizations and the chemical concepts, such as electron affinity (A), ionization potential (I), energy gap, electronegativity (χ) and hardness (η). The reactivity indices were found using the molecular system energy calculations, considering the energy E as a function of the number of electrons N, and a quadratic interpolation between the points E(N . 1), E(N), and E(N + 1).

2.1.2 Thermochemical properties

As a result of the vibrational analysis calculation, with a previous optimization of the geometry, the thermodynamic properties can be obtained using the electronic energy of the molecular systems, trying to get quantitative estimates of the studied chemical process properties. The thermochemical properties of the different reaction components were calculated at molecular level, using the DMol3 module of the Materials Studio Software (BIOVIA, 2015). In this case, reactants and products were optimized, then the vibrational contributions were obtained to reach the molecule electronic energy and the corresponding thermal corrections to find the energy of formation and, finally, calculate ΔE of the reaction. The methodology used in this section was the hybrid functional B3LYP (Becke, 1993) and the basis set DND (Delley, 1990, 2000).

Once the reaction energy was obtained by the change in energy between products and reactants, the equilibrium constant (Kp) was calculated by Eq. 4 for each reaction (Chang, 2010).

$$Kp = e^{-\Delta G/RT} \tag{4}$$

where ΔG is the Gibbs free energy, R is the gas constant and T is the absolute temperature.

The free energy of activation ($\Delta G^{\#}$) was found from the difference between the reactants and the activated complex by the Eyring equation (Eq. 5), then the reaction rate of each reaction was calculated.

$$K = \frac{K_B T}{h} e^{-\Delta G^{\#}/RT} \tag{5}$$

where K is the velocity constant, K_B is the Boltzmann's constant, and h is the Planck's constant.

2.2 *Experimental procedure*

Commercial silica sand (99.0-99.9% crystalline SiO_2) was used in this work to synthesize sodium metasilicate, which was obtained in molar proportions. A commercial sodium metasilicate (industrial-grade powder form) sample was used for comparative purposes. Three reactants: $NaHCO_3$ (99.7-100.0% powder form), Na_2CO_3 (99.3% powder form), and NaOH (97.0% pearl form) were separately used and mixed stoichiometrically with silica sand, Eqs. (1)-(3). A homogenous mixture of silica sand and a reactant was obtained using a SPEX 8000M mixer/mill in air for 5 min. Thermogravimetric analysis (TGA) and differential thermal analysis (DTA) were performed to study the behavior of the bicarbonate (Eq. 1) and carbonate (Eq. 2) reactions; the study was carried out between 25 and 1100 ºC in air using a heating rate of 10 ºC/min. The sodium hydroxide reaction (Eq. 3) was not performed to avoid corrosion in the TGA/DSC equipment. Bulk materials were processed in an Electra furnace operated at 950 ºC for the bicarbonate and carbonate reactions, using a heating rate of 10 ºC/min and a residence time of 2 h. The products were cooled under natural heat exchange conditions inside the furnace. For the sodium hydroxide reaction, the material was processed at 350 ºC in the same furnace under the conditions mentioned above. The studies were intended to be as similar to those developed by computational analysis. The X-ray diffraction (XRD) was carried in a Bruker D8 Advance diffractometer (λ = 0.15406 nm). Analyses by Raman spectroscopy were performed using a Horiba Xplora One Raman spectrometer (532-nm laser, 100x optic lens). In addition, analysis by Fourier transform infrared (FTIR) spectroscopy were achieved using a Perkin Elmer FT-IR System spectrum GX.

3 Results and discussion

3.1 *Computational analysis*

3.1.1 *Electronic properties*

Fig. 1 shows the optimized geometry of all reactants and products involved in the different reactions. The characterization of the molecular systems allowed to calculate the properties of reactants and products, which are summarized in Table 1.

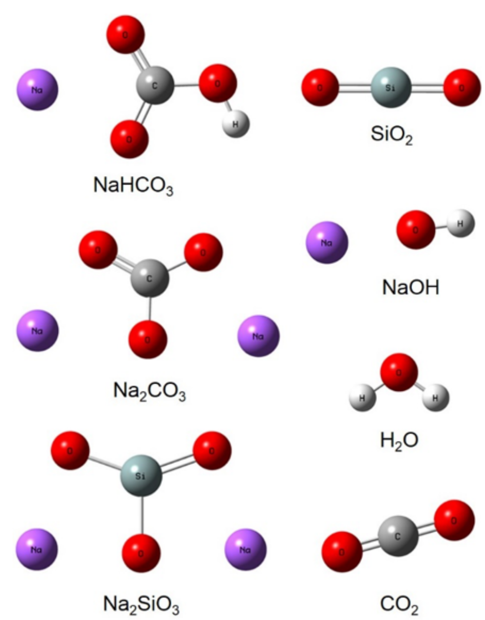

Fig. 1. Optimized geometries of reactants and products calculated with M062X/LanL2DZ.

Table 1. Electronic properties of molecular systems involved in the reactions.

Molecule	Dipolar moment (D)	Electron affinity (eV)	Ionization potential (eV)	Electronegativity (eV)	Chemical hardness (eV)	Gap (eV)
$NaHCO_3$	7.26	0.11	9.25	4.68	9.14	10.89
SiO_2	0.01	1.22	12.43	6.82	11.21	8.45
Na_2CO_3	10.51	-0.09	6.46	3.19	6.55	8.04
NaOH	5.71	0.08	7.61	3.84	7.53	5
Na_2SiO_3	9.45	-0.05	8.84	4.4	8.89	7.01
CO_2	0	-2.98	13.94	5.48	16.92	13.33

As can be seen in Table 1, the dipolar moment is canceled in molecules with linear geometry such as SiO_2 and CO_2. Reactivity parameters, including the electron affinity and ionization potential, allow to predict that Na_2CO_3, Na_2SiO_3 and CO_2 are in their maximum oxidation state, and therefore these compounds cannot accept more electrons. The electrons in these molecules are expelled instantly in the absence of new ions (Lewars, 2003). Energetically speaking, CO_2 is the most stable molecule, which requires the largest energy to react or to give up its electrons.

The electronegativity and chemical hardness were obtained to assess the intramolecular activity or selective sites of a system. According to these properties, the SiO_2 and CO_2 are the molecules with the highest stability, which is attributed to their markedly large electronegativity. The gap energy or energy difference between highest occupied molecular orbitals (HOMO) and lowest unoccupied molecular orbitals (LUMO) was in all cases over 5 eV. This means that they are not conducting systems, even for SiO_2, an intrinsic semiconductor as it is known.

3.1.2 Thermochemical properties

Reactants and products were optimized and their energy was used to calculate the Gibbs free energy of reaction in the three chemical reactions proposed. The equilibrium constant Kp was determined using Eq. 4, whose results are presented in Table 2. All reactions are endothermic and require a driving force to take place. From the Kp values we can conclude that the oxi/redox reaction to obtain sodium metasilicate using sodium hydroxide is accomplished relatively easy or effortlessly. Therefore, these results suggest that the bicarbonate reaction should be performed experimentally. However, for first-order processes, the fastest reactions cannot exceed the rates of molecular vibrations or bond-rotations and thus there is an upper limit of approximately 10^{12} s^{-1} for rate constants (Sauer, Solomon, & Baker, 2001). Consequently, the suitable reaction to obtain sodium metasilicate is by using sodium carbonate as a reactant.

In order to obtain the free energy of activation ($\Delta G^{\#}$), we used the structure of the reactants, products and the activated complex optimized. With the $\Delta G^{\#}$ value and by the Eyring equation (Eq. 5), the reaction rate of each chemical reaction was calculated. The results for reaction rates showed in Table 3 are not reliable values. All calculations exceed the upper limit (10^{12} s^{-1}) for the magnitudes of first-order and second-order rate constants.

3.2 Experimental results

Fig. 2a shows TGA and DTA results of the bicarbonate reaction (Eq. 1) behavior and Fig. 2b of that of the carbonate reaction (Eq. 2).

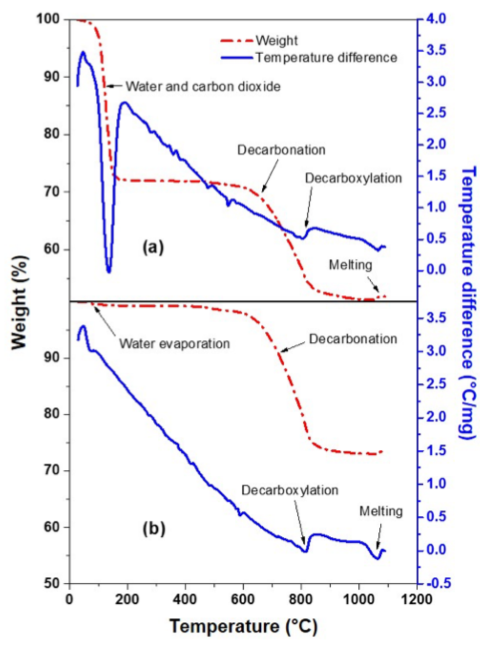

Fig. 2. TGA-DTA thermograms: (a) bicarbonate and (b) carbonate reactions.

Table 2. Reaction energies and equilibrium constants of the chemical reactions.

Reaction	**Energy of reactants (Ha)**	**Energy of products (Ha)**	**Gibbs free energy of reaction (kcal/mol)**	**Kp**
Bicarbonate	-1359	-1358.97	20.93	2.21×10^{15}
Carbonate	-1079.29	-1079.27	12.52	1.52×10^{9}
Sodium hydroxide	-960.61	-960.54	48.5	3.74×10^{35}

Bicarbonate reaction exhibits a high weight loss (28 wt%) from 100 ºC to about 150 ºC, which corresponds to water evaporation. At the same temperature range, the carbonate reaction shows a loss of 0.7 wt% of adsorbed water. This huge difference is because in the bicarbonate reaction, the hydrogen of the $NaHCO_3$ is combined with oxygen for producing H_2O, in addition to CO_2, as per Eq. 6.

$$2\,NaHCO_3(s) \xrightarrow{\Delta} Na_2CO_3(s) + H_2O(g) + CO_2(g) \tag{6}$$

The decarbonation stage for both reactions takes place between 600 and 850 ºC. The bicarbonate reaction is responsible for a weight loss of 21 wt% and carbonate reaction for 24 wt%. After the decarbonation, the forming products are sodium oxide and carbon dioxide, according to Eq. 7.

$$Na_2CO_3(s) \xrightarrow{\Delta} Na_2O(s) + CO_2(g) \tag{7}$$

Based on the DTA curves, we can identify a decarboxylation at 800 ºC and melting at 1060 ºC. The molten product is not favorable because the material strongly adheres to the crucible walls and then a thermic shock is necessary to unstick the material, with the subsequent need of reducing the particle size, which leads to greater losses of energy and time.

Fig. 3 presents the XRD patterns and Rietveld refinements of the three reactions. The bicarbonate reaction product (Fig. 3a) displays characteristic reflections of Na_2SiO_3 (JCPDS 00-016-0818 standard). Although other signals can be seen with lower intensity in the region corresponding to SiO_2 (JCPDS 00-046-1045, alpha quartz). This in turn implies that not all the silicon dioxide reacted with sodium bicarbonate. The Rietveld refinement indicates that 96% corresponds to the Na_2SiO_3 phase and the other 4% to that of the SiO_2. This incomplete reaction may be due to the dehydration that $NaHCO_3$ experiences during heating, as seen in the TGA analysis (Fig. 2a), where a water weight loss of 28% was calculated for the temperature range of 100-150 ºC. Our results match well with those found by Pasquali *et al*. (Pasquali, Bettini, & Giordano, 2007), who reported that the thermal decomposition of $NaHCO_3$ occurs between 50 ºC and 170 ºC generating H_2O, CO_2 and sodium carbonate (Eq. 6). Hartman *et al*. (Hartman, Svoboda, Pohořelý, & Šyc, 2013) detailed that $NaHCO_3$ begins to decompose at 82 ºC, reaching complete decomposition at 165 ºC. This fact must be taken into account for achieving a complete transformation from $NaHCO_3$ into Na_2SiO_3. The product of the carbonate reaction (Fig. 3b) matches well with the characteristic reflections of Na_2SiO_3; the SiO_2 phase is not appreciated. Therefore, the only product identified by the Rietveld refinement is Na_2SiO_3. Finally, the product of the sodium hydroxide reaction (Fig. 3c) shows intense characteristic peaks of SiO_2, meaning that the reaction was not completed; this is, the whole transformation to Na_2SiO_3 was not favored. The Rietveld refinement results indicate that the product contains 60% of SiO_2 and 40% of Na_2SiO_3.

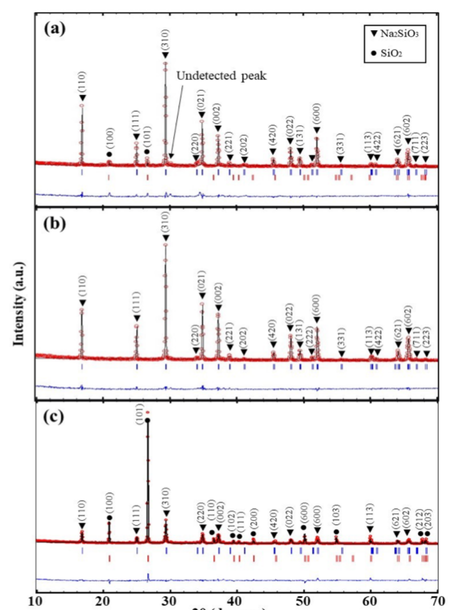

Fig. 3. XRD pattern Rietveld refinement of Na_2SiO_3 obtained by the three different reactions: a) bicarbonate, b) carbonate, and c) sodium hydroxide.

Table 3. Activation energies and reaction rates.

Reaction	Transition state energy (Ha)	Energy barrier (kcal/mol)	K
Bicarbonate	-1358.96	25.4	2.60×10^{31}
Carbonate	-1079.29	3.69	3.17×10^{15}
Sodium hydroxide	-960.53	55.06	3.69×10^{13}

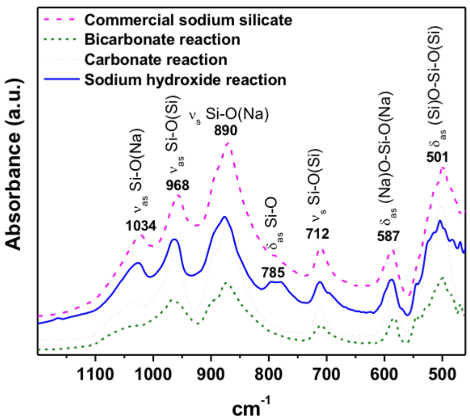

Fig. 4. Infrared spectra of Na_2SiO_3 obtained by different reactions.

With these results, we can infer that the carbonate reaction (Eq. 2) is the best reaction to get a higher quantity of crystalline Na_2SiO_3. This information complements the results obtained by the computational analysis, in which it was anticipated that the carbonate reaction would be the most effective reaction.

Fig. 4 shows the FTIR spectra of the products from the three reactions. The spectra obtained are similar to those reported by Halasz *et al*. (Halasz, Agarwal, Li, & Miller, 2007) and Lazarev (Lazarev, 1995) for anhydrous Na_2SiO_3. The bands observed at 1034 and 968 cm^{-1} belong to ν_{as} SiO(Na) and ν_{as} SiO(Si), respectively; attached to the oxygen atoms the next linking atoms are shown in parentheses. The symbol ν refers to the stretching and δ to deformation (bending, twisting, and rocking) vibrations; the indexes "*s*" and "*as*" refer to symmetric and asymmetric motions, respectively. The bands at 890 and 712 cm^{-1} correspond to ν_s Si-O(Na) and ν_s Si-O(Si) and, finally, those located at 785, 587 and 501 belong to δ_{as} Si-O, δ_{as} (Na)O-Si-O(Na) and δ_{as} (Si)O-Si-O(Si), respectively. The study reveals that the stretching Si-O vibrations (ν) appear at higher wavenumbers than the less energetic deformation vibrations (δ); the asymmetric vibrations (ν_{as}, δ_{as}) usually have higher energies than their symmetric pairs (ν_s, δ_s). The main difference between the signals of the Na_2SiO_3 samples is the band observed at 785 cm^{-1}, which belongs to the Si-O bending and is the characteristic band of quartz (SiO_2) (Brawer & White, 1975; Salh, 2011). This signal only appears for the product of the sodium hydroxide reaction, in which a greater amount of quartz was detected in X-ray diffraction by the Rietveld refinement.

Fig. 5 shows the Raman spectra of the synthesized products, which complement the X-ray diffraction studies, since they are sensitive to the general structure of the glass network. Based on the Brawer's study (Brawer & White, 1975), the products of the bicarbonate and carbonate reactions are crystalline, which is evidenced by the presence of narrow bands in the region from 500 to 1100 cm^{-1} and the defined bands in the region from 100 to 400 cm^{-1}. In the case of the sodium hydroxide reaction, the shape of the Raman spectrum is similar to that of a glass. This is identified by the fuzzy bands and their respective shift to lower frequencies in the region from 150 to 400 cm^{-1}. Some bands have been identified by Halasz *et al*. (Halasz *et al*., 2007). For instance, the band at 974 cm^{-1} belongs to the Si-O(Si) asymmetric stretching vibration. The bands located at 756 cm^{-1} and 592 cm^{-1} correspond to (H)O-Si-O(H) and (Na)O-Si-O(Na), respectively. Both bands present an asymmetric bending vibration.

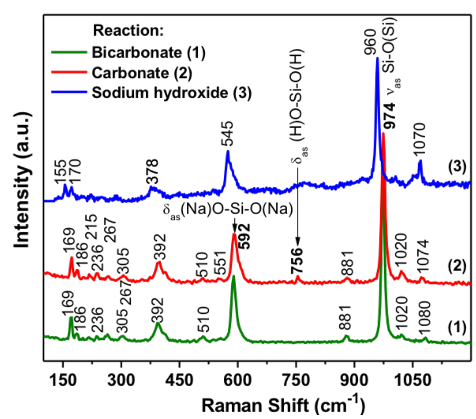

Fig. 5. Raman spectra of Na_2SiO_3 obtained by different chemical routes.

Conclusions

Three different routes to produce granular crystalline sodium metasilicate were studied by computational analysis and experimentally. $NaHCO_3$, Na_2CO_3 and NaOH were separately used as reactants in combination with silica sand in stoichiometric concentrations. The behavior of the reactions, as well as their products, were followed by different techniques. The results of both studies, through a systematic study of the three reactions studied in this work, allow to conclude that the best route to produce Na_2SiO_3 is by reacting sodium carbonate with silicon dioxide:

$$Na_2CO_3(s)SiO_2(s) \xrightarrow{\Delta} Na_2SiO_3(s) + CO_2(g) \quad (8)$$

The efficiency of this reaction was demonstrated by XRD and the Rietveld refinement; the analysis was complemented by infrared and Raman spectroscopies, which confirmed the presence of a crystalline sodium metasilicate. According to the thermal analysis results, the adequate temperature to accomplish the synthesis is between 870 ºC and 1000 ºC to produce a granular product.

Acknowledgements

This work was supported by Grupo Cementos de Chihuahua, Department of Mechanical Engineering Technology at the University of Houston and Centro de Investigacion en Materiales Avanzados. ATO thanks to CONACYT for their scholarship (grant number 445419). Thanks are due to D. Lardizabal-Gutierrez and L. de la Torre-Saenz for their laboratory assistance.

References

Becke, A. D. (1993). Density-functional thermochemistry. III. The role of exact exchange. *The Journal of Chemical Physics 98*, 5648-5652.

BIOVIA. (2015). Materials Studio 7.0, Visualizer, DMoI3 module, Accelrys Inc. San Diego.

Brawer, S. A., & White, W. B. (1975). Raman spectroscopic investigation of the structure of silicate glasses. I. The binary alkali silicates. *The Journal of Chemical Physics 63*, 2421-2432.

Brown, J. R., & Limited, F. (1994). *Foseco Foundryman's Handbook*. Butterworth-Heinemann.

Bulatovic, S. M. (2007). *Handbook of Flotation Reagents - Chemistry, Theory and Practice*, Volume 2 - Flotation of Sulfides Ores: Elsevier.

Chang, R. (2010). *Físico-Química* 3.ed.: Para as Ciências Químicas e Biológicas: AMGH Editora.

Daramola, M. O., Nkazi, D., & Mtshali, K. (2015). Synthesis and evaluation of catalytic activity of calcined sodium silicate for transesterification of waste cooking oil to biodiesel. *International Journal of Renewable Energy Research (IJRER) 5*, 517-523.

Delley, B. (1990). An all-electron numerical method for solving the local density functional for polyatomic molecules. *The Journal of Chemical Physics 92*, 508-517.

Delley, B. (2000). From molecules to solids with the DMol3 approach. *The Journal of Chemical Physics 113*, 7756-7764.

Evcin, A. (2011). Investigation of the effects of different deflocculants on the viscosity of slips. *Scientific Research and Essays 6*, 2302-2305.

Frisch, M. J., Trucks, G., Schlegel, H., Scuseria, G., Robb, M., Cheeseman, J., … Petersson, G. (2009). Gaussian 09, revision A. 1. Gaussian Inc., Wallingford, CT.

Halasz, I., Agarwal, M., Li, R., & Miller, N. (2007). Vibrational spectra and dissociation of aqueous Na_2SiO_3 solutions. *Catalysis Letters 117*, 34-42.

Hartman, M., Svoboda, K., Pohořelý, M., & Šyc, M. (2013). Thermal decomposition of sodium hydrogen carbonate and textural features of its calcines. *Industrial & Engineering Chemistry Research 52*, 10619-10626.

Hohenberg, P., & Kohn, W. (1964). Inhomogeneous electron gas. *Physical Review 136*, B864-B871.

Lazarev, A. N. (1995). *Vibrational Spectra and Structure of Silicates*. Springer.

Lewars, E. G. (2003). *Computational Chemistry: Introduction to the Theory and Applications of Molecular and Quantum Mechanics*. Springer.

López, C., García, A., Ríos, M., Pérez, M., Román, J., García, L., & Villarroel, A. (2018). Escalamiento piloto de la síntesis de zeolita NaA a partir de geles aluminosilicatos obtenidos con materiales industriales venezolanos no tratados. *Revista Mexicana de Ingeniería Química 17*, 75-86.

NOM. (2009). Silicato de sodio o potasio para uso industrial Norma mexicana (Vol. NMX-K-240-SCFI-2009). México, D.F.: NMX-K-240-SCFI.

Parr, R. G. (1980). Density Functional Theory of Atoms and Molecules. In K. Fukui & B. Pullman (Eds.), *Horizons of Quantum Chemistry: Proceedings of the Third International Congress of Quantum Chemistry Held at Kyoto, Japan*, October 29 - November 3, 1979 (pp. 5-15). Dordrecht: Springer Netherlands.

Pasquali, I., Bettini, R., & Giordano, F. (2007). Thermal behaviour of diclofenac, diclofenac sodium and sodium bicarbonate compositions. *Journal of Thermal Analysis and Calorimetry 90*, 903-907.

Rehren, B. E. V. (2000). Mexico Patent No. 198108.

Salh, R. (2011). Defect related luminescence in silicon dioxide network: a review. In: *Crystalline Silicon - Properties and Uses* (pp. 135-172), S. Basu (Ed.), InTech.

Sauer, B., Solomon, F., & Baker, T. (2001). 7.51 Graduate Biochemistry. Fall 2001. Massachusetts Institute of Technology: MIT OpenCourseWare. Retrieved from https://ocw.mit.edu

Schaefer, H. F. (2013). *Methods of Electronic Structure Theory*. Springer US.

Schimmel, G. (1993a). United States Patent No. 5229095.

Schimmel, G. (1993b). United States Patent No. 5183651.

Stratmann, R. E., Scuseria, G. E., & Frisch, M. J. (1998). An efficient implementation of time-dependent density-functional theory for the calculation of excitation energies of large molecules. *The Journal of Chemical Physics 109*, 8218-8224.

Torres-Ochoa, A., Osornio-Rubio, N., Jiménez-Islas, H., Navarrete-Bolaños, J., & Martínez-González, G. (2019). Synthesis of a geopolymer and use of response surface methodology to optimize its adhesion to red brick for improve the internal coatings in burner kilns. *Revista Mexicana de Ingeniería Química 18*, 361-373.

Zhao, Y., & Truhlar, D. G. (2008). Density functionals with broad applicability in chemistry. *Accounts of Chemical Research 41*, 157-167.